AQUARIUS RADIOMETER
RFI DETECTION, MITIGATION AND IMPACT ASSESSMENT

Christopher Ruf[1], David Chen[1], David Le Vine[2], Paolo de Matthaeis[2], Jeffrey Piepmeier[2]

1. University of Michigan, Ann Arbor, MI USA
2. NASA Goddard Space Flight Center, Greenbelt, MD USA

1. INTRODUCTION

The Aquarius/SAC-D satellite was launched on 10 June 2011 into a sun-synchronous polar orbit and the Aquarius microwave radiometers [1] became operational on 25 August 2011. Since that time, it has been measuring brightness temperatures at 1.4 GHz with vertical, horizontal and 3rd Stokes polarizations . Beginning well before the launch, there has been the concern that Radio Frequency Interference (RFI) could have an appreciable presence. This concern was initiated by, among other things, its prevalence in both early [2] and more recent [3,4] aircraft field experiments using 1.4 GHz radiometers, as well as by the strong RFI environment encountered during the recent ESA SMOS mission, also at 1.4 GHz [5]. As a result, a number of methods for RFI detection and mitigation have been developed and tested. One in particular, "glitch detection" and "pulse blanking" mitigation has been adapted for use by Aquarius [6, 7]. The early on-orbit performance of the Aquarius RFI detection and mitigation algorithm is presented here, together with an assessment of the global RFI environment at 1.4 GHz which can be derived from the Aquarius results.

2. DETECTION AND MITIGATION ALGORITHM

The measurement sampling rate of the radiometer is significantly higher than the Nyquist spatial sample rate dictated by its antenna beam width in order to enhance its ability to detect and mitigate anticipated forms of RFI [7]. When RFI is not present, these short subsamples are averaged together to reduce radiometric noise. When RFI is detected in some of the subsamples, they are removed from the average in ground processing. Oversampling in this way is believed to be especially helpful for overcoming pulsed RFI such as is are produced by large air traffic control and early warning radars. Ground processing of the Aquarius data detects the presence of RFI by examining the variance of the subsamples and flagging those which deviate from their neighbors more than can be confidently explained by normal radiometric noise statistics [8]. This approach to RFI detection and mitigation has been validated previously in ground-based and airborne campaigns [3].

3. FIRST DETECTION AND MITIGATION RESULTS

Histograms of the H-pol brightness temperature before (designed TA) and after (designed TF) the mitigation algorithm is applied are shown on the right in Fig. 1 for land-only observations and in Fig. 2 for ocean-only observations. Histograms of the difference between the two (*i.e.* TA – TF) are shown for the land-only and ocean-only observations on the right. Fig. 1 (left) illustrates the very high probability of occurrence of RFI-contaminated measurements over land (the blue TA bars), which is consistent with the environment experienced by SMOS. It also shows that, the mitigation algorithm has successfully removed almost allof the non-physically high brightness temperature values.

The histogram of the difference (TA – TF) shown on the right in Fig. 1 illustrates both the RFI and the "false alarm" occurrences of clean measurements that were mistakenly identified as RFI-contaminated. The high probability of (TA – TF) values near zero is likely due primarily to those false alarms. Higher values are likely due to RFI.

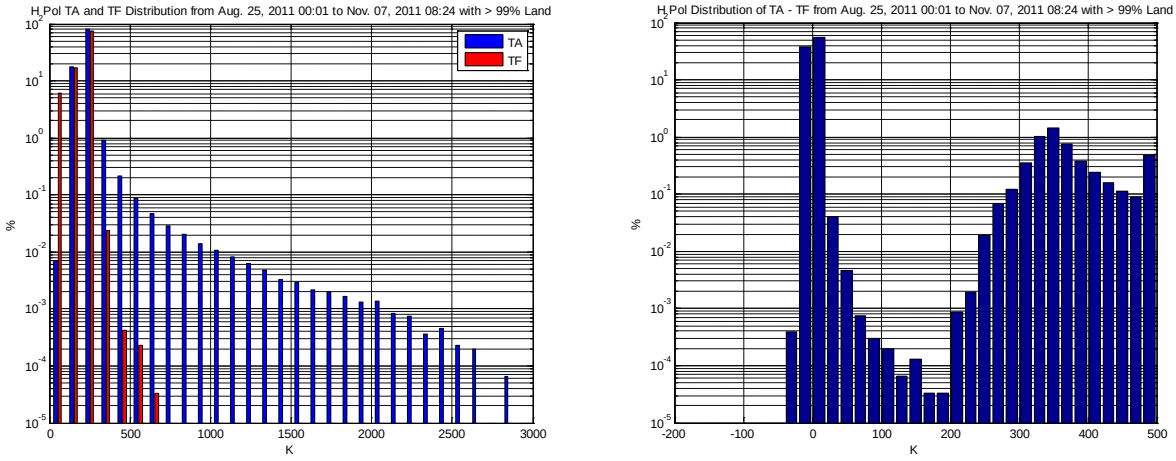

Figure 1: (a) Histograms of measured H-pol brightness temperature (TA, blue) and brightness temperature after RFI mitigation (TF, red) for over-land observations. (b) Histogram of the difference (TA – TF) shows the RFI environment at high values and the probability of occurrence of false alarms at low values. Values greater than 500 K are included in the 500 K bin.

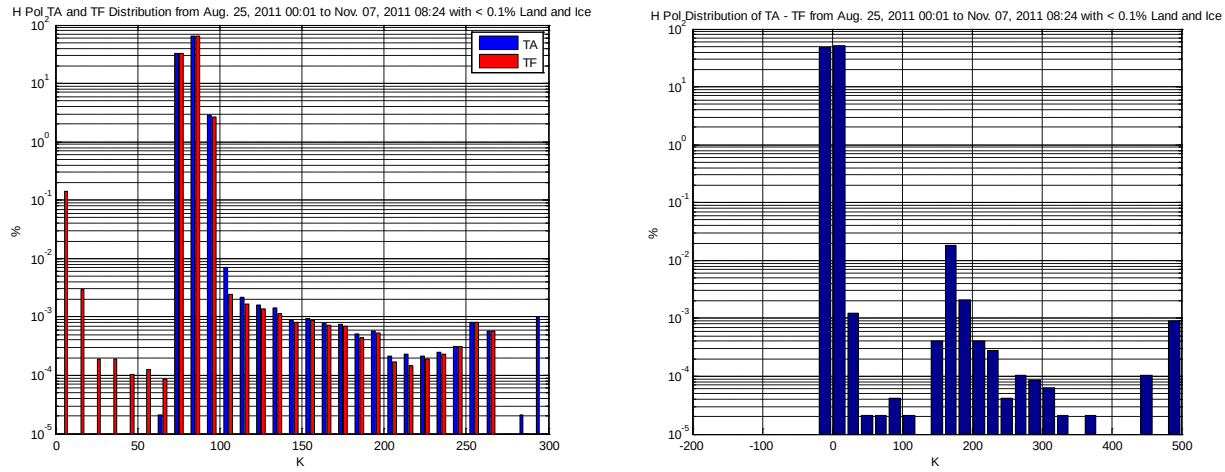

Figure 2: Similar plots as in Fig. 1 for the over-ocean observations. In (a), TF values below ~60 K indicate problems with the mitigation algorithm. They happen infrequently and are flagged and removed at a later processing stage.

Fig. 2 shows data over the ocean in the same format as Fig 1. Comparison with Fig shows that, as expected, there is much less RFI over ocean. However, it is not entirely absent (e.g. values greater than 100K in the panel on the left). The occurrences of TF with values below ~ 60K on the left panel illustrate occasional problems with the mitigation algorithm, as such values are physically unrealizable over the ocean. This happens only infrequently and the occurrences are flagged and removed at later processing stage. However, the problem is currently being studied and will be corrected. Work is underway to tune the algorithm to reduce the false alarm rate, especially over the ocean, and to remove problems such as the low values (Fig 2, left) and residual large values (Fig 1, left) which suggest missed RFI.

4. FIRST RFI CHARACTERIZATION RESULTS

The geographic distribution of prevalent RFI over the ocean is illustrated in Fig. 3 (left), which shows a "peak hold" RFI map for 25 Aug – 24 Dec 2011. To create this map, a climatology of the average RFI-free brightness temperature is first derived by averaging over all observations for which TA (raw observations) and TF (RFI mitigated observations) are the same. The deviation of TA from the climatological average is then noted for every observation over a period of time, and the largest deviation is plotted in the peak hold map. A histogram of the values in the peak hold map is shown on the right in Fig. 3. It illustrates the probability of occurrence if RFI over the ocean as a function of the strength of the RFI.

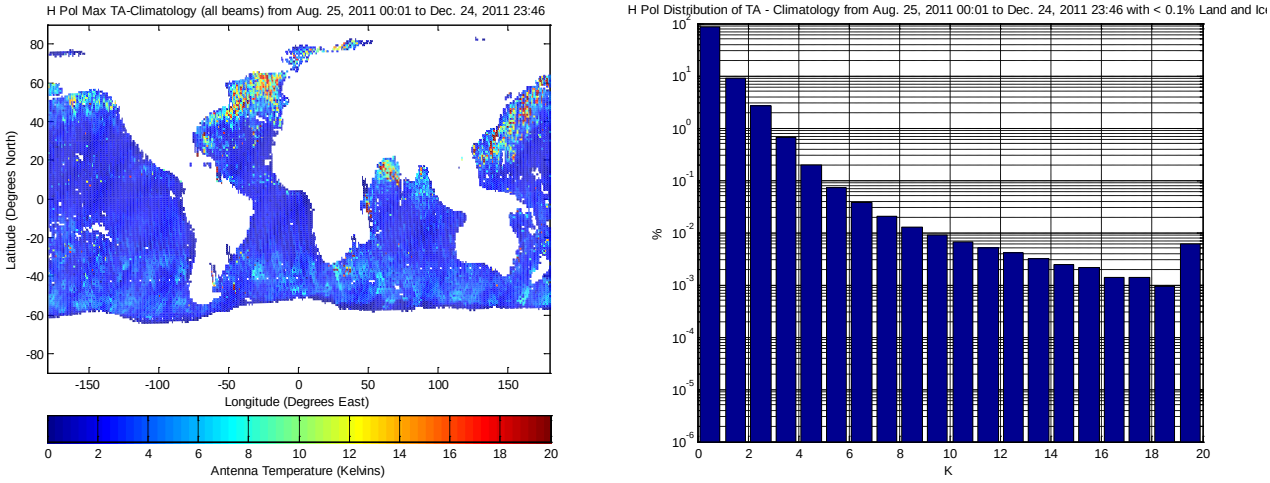

Figure 3: (a) Peak hold RFI map of the largest deviation of brightness temperature from the average RFI-free value over the period 25 Aug – 24 Dec 2011 highlights the regions of prevalent RFI over the ocean. (b) Histogram of the samples in Fig. 3a.

5. ACKNOWLEDGMENTS

Data were furnished through the NASA/CONAE Aquarius/SAC-D Project.

6. REFERENCES

[1] Le Vine, D.M.; Lagerloef, G.S.E.; Colomb, F.R.; Yueh, S.H.; Pellerano, F.A., "Aquarius: An Instrument to Monitor Sea Surface Salinity From Space," *IEEE Trans. Geoscience and Remote Sensing*, 45(7), 2040-2050, July 2007.

[2] Le Vine, D.M., "ESTAR Experience with RFI at L- band and Implications for Future Passive Microwave Remote Sensing from Space," Proc. IGARSS 2002, Toronto, Canada.

[3] Misra, S., P. N. Mohammed, B. Guner, C. S. Ruf, J. R. Piepmeier, and J. T. Johnson, "Microwave radiometer radio-frequency interference detection algorithms: A comparative study," Geoscience and Remote Sensing, IEEE transactions on, vol. 47, pp. 3742-3754, 2009.

[4] Skou, N., S. Misra, J. E. Balling, S. S. Kristensen, and S. S. Sobjaerg, "L-Band RFI as Experienced During Airborne Campaigns in Preparation for SMOS," Geoscience and Remote Sensing, IEEE Transactions on, vol. 48, pp. 1398-1407, 2010.

[5] Camps, A., J. Gourrion, J. M. Tarongi, A. Gutierrez, J. Barbosa, and R. Castro, "RFI analysis in SMOS imagery," IEEE Geoscience and Remote Sensing Symposium (IGARSS), Proceedings, 2010, pp. 2007-2010.

[6] Niamsuwan, N., J. T. Johnson, and S. W. Ellingson, “Examination of a simple pulse blanking technique for RFI mitigation” *Radio Science*, vol. 40, June 2005.

[7] Piepmeier, J. and F. Pellerano, “Mitigation of Terrestrial Radar Interference in L-Band Spaceborne Microwave Radiometers,” *Proc. IEEE Int. Geoscience and Remote Sensing Symposium (IGARSS)*, Denver, CO, pp. 2292-2296, July 30-Aug 4, 2006.

[8] Misra, S., and C. Ruf, “Detection of Radio-Frequency Interference for the Aquarius Radiometer,” *IEEE Transactions Geoscience Remote Sensing*, 46(10), 2008.